TEMPERATURE EFFECT ON THE MECHANICAL PROPERTIES OF LINER MATERIALS USED FOR TYPE IV HYDROGEN STORAGE TANKS

Li, Y.F.[1], Zheng, J. Y.[2 *] and Li, Q.N.[3]
[1] Institute of Process Equipment, Zhejiang University, Hangzhou, 310027, China, wjslyf@zju.edu.cn
[2] Institute of Process Equipment, Zhejiang University, Hangzhou, 310027, China, jyzh@zju.edu.cn
[3] Institute of Process Equipment, Zhejiang University, Hangzhou, 310027, China, 740555752@qq.com

ABSTRACT

Type IV hydrogen storage tanks play an important role in hydrogen fuel cell vehicles (HFCVs) due to their superiority of lightweight, good corrosion and fatigue resistance. It is planned to be used between -40℃ and 85℃ at which the polymer liner may have a degradation of mechanical properties and buckling collapse. This demand a good performance of liner materials in that temperature range. In this article, the temperature effect on mechanical properties of polyamide 6 (PA6) liner material, including specimens with weld seam was investigated via the stress-strain curve (S-S curve), macroscopic and microscopic morphology. Considering that the mechanical properties will change after the liner molding process, this test takes samples directly from the liner. Results show that the tensile strength and tensile modulus increased by 2.46 times and 10.6 times, respectively, with the decrease of temperature, especially in the range from 50℃ to -90℃. For the elongation at break and work of fracture, they do not monotonously increase with the temperature up. Both of them reduce when the temperature rises from 20 ℃ to 50 ℃, especially for the work of fracture, decreasing by 63%. The weld seam weakens the mechanical properties, and the elongation at break and work of fracture are more obvious, which are greater than 40% at each temperature. In addition, the SEM images indicate that the morphology of fracture surface at -90 ℃ is different from that at other temperatures which is a sufficient evidence of toughness reducing in low temperature.

1.0 INTRODUCTION

Nowadays, with the gradual depletion of non-renewable energy resources like fossil fuel, the development and utilization of low carbon and renewable energy resources become more and more urgent [1, 2]. As one of the alternative secondary energy, hydrogen has been widely used in transportation, industrial energy and building cooling heating power (BCHP) because of its great feature of no greenhouse gas emission [3, 4]. In automotive industry, many international companies such as Toyota Motor, Honda Motor, Hyundai Motor and Benz Motor make great effort to develop hydrogen fuel cell vehicles (HFCVs) [5-7]. Currently, hydrogen storage tank is the good solution for on-board hydrogen storage. There are two types of hydrogen storage tanks commonly used for HFCVs due to their good strength, light stiffness-weight ratio, excellent corrosion and fatigue resistance: composite pressure vessels with metal liner (Type III hydrogen storage tanks) and composite pressure vessels with plastic liner (Type IV hydrogen storage tanks). Type III and type IV hydrogen storage tanks each have their own advantages, while in recent years type IV hydrogen storage tanks get more attention for its unique features like lightweight and low-cost.

During the service period of hydrogen storage tank, it may experience multiple hydrogen refueling and discharging process. To evaluate the on-road performance of hydrogen storage tank under refueling and discharging cycle, hydrogen gas cycling test has been explicitly requested as a type testing by relevant regulations, codes and standards such as EC RUGULATION 406, UN GTR 13, ISO 19881, SAE J2679, ANSI HGV 2[8]. Under the hydrogen gas cycling test, the gas temperature in the tank will change dramatically due to the following reasons: (1) the hydrogen is compressed and decompressed in the limited tank space; (2) the Isentropic expansion of hydrogen occurs at the nozzle with the inverted Joule-Thomson effect. (3) the conversion between the kinetic energy and internal energy of

hydrogen. In the fast refueling process, with the hydrogen precooling below 0℃, the maximum temperature in the tank can be controlled below 85 ℃, while in the case of no pre-cooling, the maximum temperature will exceed 85 ℃ [9, 10]. De Miguel et al. [11, 12] simulated the defueling process of HFCVs in service through hydrogen release tests on type III and IV hydrogen storage tank. The results showed that the internal temperature decreased during the defueling process, and when the vehicle accelerates, the internal temperature even dropped below -40 ℃. In addition, the temperature change of type IV gas cylinder is more severe than that of type III gas cylinder. Those thermos-mechanical stress leads to the degradation of mechanical properties of plastic liner materials such as HDPE and PA, which increases the risk of buckling collapse. Therefore, it is very important to study the temperature effect on the mechanical properties of plastic liner materials.

In recent years, a lot of experimental and numerical study has been performed to investigate the temperature rise of hydrogen storage tank during the fast refuelling [13-15]. However, the studies on the temperature effect on the mechanical properties of plastic materials used for the liner is less reported. K. Baek et al. [16] obtained the stress-strain curves of uniaxial tension test of polyamide 66 under 5 ambient temperatures (240K, 270K, 300K, 330K and 355K) by molecular dynamics (MD) simulations. The obvious dependency of temperature on the mechanical properties were showed by simulation results and remarkable degradations of the mechanical properties are observed with increasing temperature. S. Felder et al. [17] conducted monotonic, cyclic, and relaxation tests of polyamide 6 during 4 ambient temperatures (23℃, 50℃, 120℃ and 160℃) to study the influence of ambient temperature on viscoelastic, elastoplastic behaviour of PA6. The experimental results showed that the temperature increase lead to thermal softening and a reduction of the hardening slopes. A.J. Cano et al. [18] conducted tensile and fracture tests under 3 temperature conditions (-50℃, 23℃ and 50℃) to study the temperature effect on the mechanical properties of polyamide 12. The results were Young's modulus and tensile strength increased with decreasing temperature and the tendency of Poisson's ratio and the elongation at break were opposite. However, in the existing research, their subject is not specific to the hydrogen storage tank and the studied temperature range cannot fully include the actual working condition.

In this paper, the temperature effect on the mechanical properties of polyamide 6 (PA6) used for liner materials of type IV hydrogen tank was studied. The specimens are directly sampled from the liner to avoid the influence of the molding process. This work also considering the wider temperature range from -90℃ to 90℃, and analyzing the weld seam effect on the mechanical properties such as tensile strength, tensile modulus, the elongation at break and work of fracture. Furthermore, SEM is used for comparing the different morphology of the fracture surface.

2.0 EXPERIMENTAL PROCEDURE

2.1 Materials

The polyamide 6 material in this paper is from the liner of a type IV hydrogen storage tank. To avoid the change of mechanical properties after the liner molding process, the test specimens are directly taken from the plastic liner. There are two weld seams on the liner from where the specimens with weld seam sampled.

2.2 Processing

The specimens were taken from the base material (BM) and the weld seam (WS) as shown in Fig.1, each with the nominal dimensions 2×5×98 mm (thickness, width, length). The length direction of the specimen is parallel to the axial direction of the plastic liner. The weld seam of WS specimen is located in the middle of the specimen.

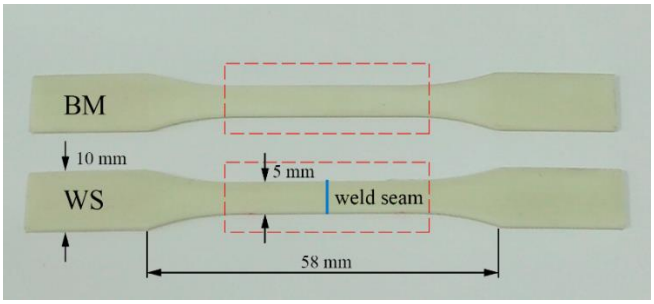

Figure 1. Base material (BM) and weld seam (WS) specimen. The red line portion shows the different area between BM and WS specimen. The blue line represents the position of weld seam.

2.3 Crystallinity and glass transition temperature measurements

The crystallinity was calculated by heating the specimen from 40℃ to 260℃ at a rate of 10 ℃·min^{-1} in nitrogen atmosphere (the flow rate was 50 ml ·min^{-1}) via differential scanning calorimetry (DSC). After determining the area of endothermic peak, ΔH, in Fig.2, the crystallinity, X_c, can be calculated by Eq. (1):

$$X_c = \frac{\Delta H}{\Delta H_0} \times 100\%, \tag{1}$$

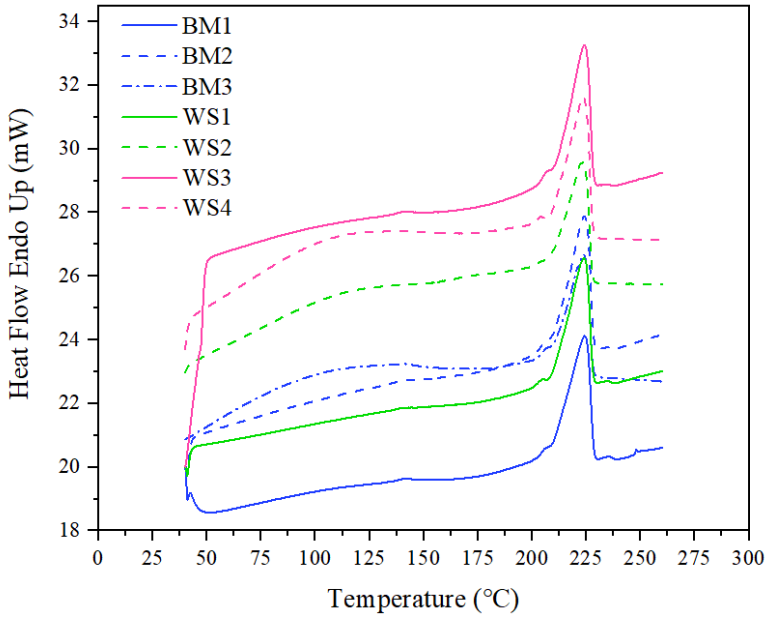

Figure 2. The endothermic transition curve of specimens

Fig.2 shows a single melting peak of 224℃ which indicates the PA6 materials belong to the α-crystal phase. Table.1 gives values of X_c calculated via Eq. (1), taking the melting enthalpy of α-crystal phase of PA6 at 100% crystallinity, ΔH_0, as 241 J ·g^{-1} [19]. There is a heat-affected zone (HAZ) in welding process. Of these seven specimens, three are base metal samples (BM1, BM2, BM3), two are close to HAZ (WS1, WS2), and the remaining two are in HAZ (WS3, WS4). The WS3 and WS4 specimen sampled close to the weld seam is impacted by the HAZ and had a higher crystallinity. This is expected to be caused by an already beginning recrystallization which makes the grain coarsened, the molecular chain closely arranged, the porosity decreasing, and no room for movement [20, 21]. Therefore, the crystallinity of HAZ is higher than other zones of the specimen. It has poor mechanical properties and cannot resist a big deformation.

Table 1. The crystallinity of specimens.

Specimens	ΔH/J g^{-1}	T_m/℃	X_c/%
BM1	48.7	224.2	20.2
BM2	50.4	224.0	20.9
BM3	47.3	223.7	19.6
WS1	46.3	223.8	19.2
WS2	46.7	223.5	19.4
WS3	54.4	224.0	22.6
WS4	55.4	223.7	23.0

The glass transition temperature (T_g) was determined by the inflection point of second heating curve from -20℃ to 250℃ at a rate of 10 ℃·min-1. From Fig.3, the T_g of PA6 materials is 51.9℃, as the mean value of T_{g1} and T_{g2}. Because the T_g measurement result is positively correlated to the heating rate [22, 23], the real value of T_g should be slightly lower than 51.9℃.

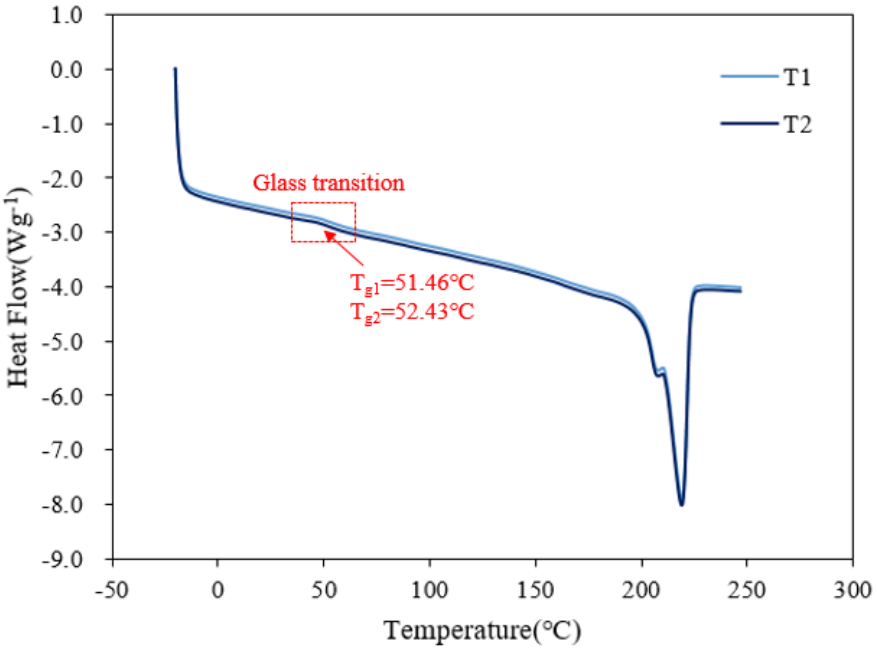

Figure 3. The second heating curve of specimens from -20℃ to 250℃

2.4 Tensile test

Tensile tests on both BM and WS specimens were conducted on universal tensile testing machine with the initial separation of 58 mm. The speed of crosshead is 1 mm/min recommended by the GB/T 1040.1 standard, giving nominal strain rate of 2.87×10^{-4} s^{-1}. The temperature effect was studied at that crosshead speed and test temperature of -90℃, -70℃, -50℃, -20℃, 20℃, 50℃, 70℃ and 90℃. In order to study the effect of weld seam on the mechanical properties of this polyamide 6, uniaxial tensile experiments of WS specimens have been carried at the same strain rate and temperatures of -70℃, -50℃ and 20℃.

Each specimen cooled by liquid nitrogen or heated by resistance wire has been held in target temperature isothermally for 30 minutes before loading. In each test temperature, at least three specimens were tested for determining an average value. The tensile force and displacement of each specimen during the whole tensile process were recorded by a computer.

3.0 RESULTS AND DISCUSSION

3.1 Stress-strain curve

The engineering stress and strain are calculated by Eq. (2) and Eq. (3):

$$\sigma = F / A_0, \tag{2}$$

$$\varepsilon = \Delta l / l_0, \tag{3}$$

where σ – engineering stress, MPa; ε – engineering strain; F – tensile force, N; A_0 – the initial area of cross section, mm^2; Δl– the displacement of crosshead, mm; l_0 – the initial distance of crosshead, mm.

The stress-strain curves of BM and WS specimens at each test temperature were showed in Fig.4. It is apparently that temperature imposes distinctive influence on the tensile process of the polyamide 6. For all specimens, the S-S curves have a similar trend without obvious yield necking process. First, the stress increases linearly with the increase of strain. The stress increases slowly when reaching the yield point demonstrating the viscous flow deformation effect. With the orientation deformation of the molecular chain, the strength of the specimen increases gradually. The stress increase after instantaneous elastic deformation of WS specimens is slower than that of BM specimens. In this process, the specimen is stretched and elongated uniformly. Finally, the specimen breaks after a long-time strain.

It is generally believed that brittle fracture occurs before the yield of material. In this case, the material only has general elastic deformation, the curve of stress-strain is nearly linear, the degree of deformation is small, the elongation at break is less than 5%, and a large number of crazing are formed during the tensile process. On the other hand, the ductile fracture occurs after the material yields, the stress-strain relationship is nonlinear, and the elongation at break is generally more than 10%. As shown in Fig.4, the elongation at break of all BM and WS specimens larger than 10%, by which, we can preliminarily determine that the fractures are all ductile.

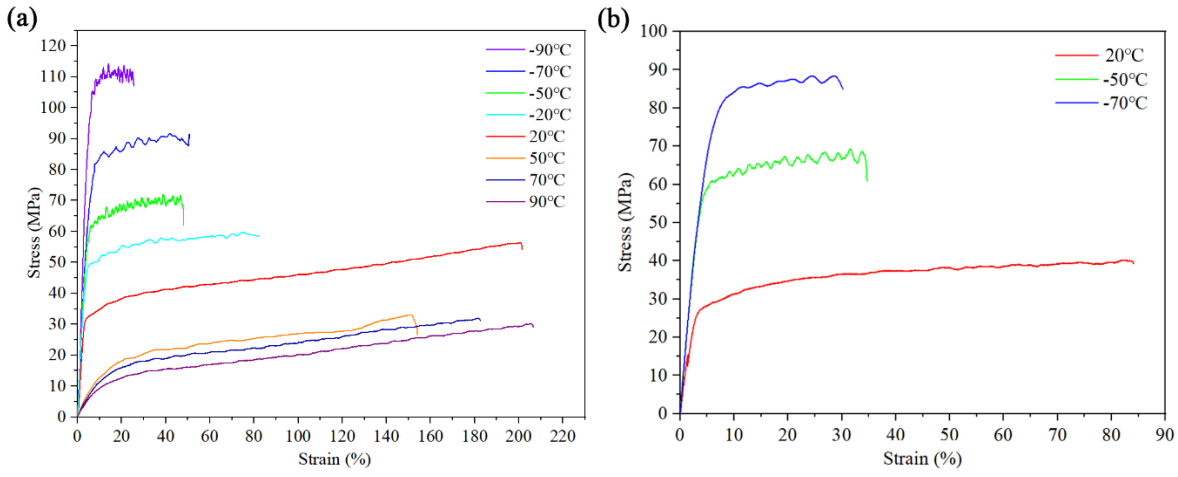

Figure 4. Stress-strain curves at each test temperature of (a) BM specimens, (b) WS specimens

3.2 Temperature effect of mechanical properties

3.2.1 Tensile strength and tensile modulus

The variation of tensile strength and tensile modulus at test temperature ranging from -90°C to 90°C has been showed in Fig.5. Tensile modulus refers to the ratio of stress to strain before yielding, and is the slope of the initial straight line in the stress-strain curve (S-S curve). It can be calculated by fitting the initial straight part of the S-S curve.

The tensile strength and tensile modulus show a similar trend with temperature increasing. As temperature rises, the tensile strength and tensile modulus decreases with fluctuations. The maximum tensile strength and tensile modulus are both at -90℃. The variation is apparent in low temperature demonstrating the mechanical strengthening effects. While at high temperature, the degradation in the tensile strength and tensile modulus was smaller. The tensile strength decreased by 37.7 MPa from -90℃ to -50℃, while only by 4.8 MPa from 50℃ to 90℃. The decrease of tensile modulus with every 20℃ up is 0.381, 0.102, 0.105, 0.331, 0.895, 0.034 and 0.023, respectively.

In addition, tensile strength and tensile modulus has a marked decrease from 20℃ to 50℃, especially for tensile modulus which reduced about an order of magnitude. This sudden reduction is related to the phase transition of the polymer chain from the glassy state to the rubbery state with temperature up, which also decreases the yield stress, causing the appearance of the liner collapse [24, 25]. This phenomenon is also proved by the T_g measured in chapter 2.3. After this transition, the tensile modulus reaches a plateau region. Based on the experimental results, the temperature effect on tensile strength and tensile modulus is significantly greater in the range from -90℃ to 50℃.

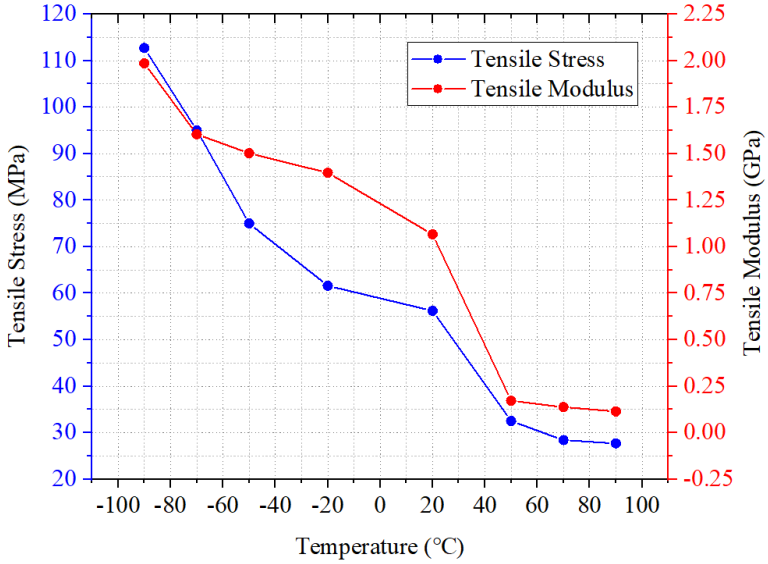

Figure 5. Curves of tensile strength and tensile modulus at temperature ranging from -90℃ to 90℃

3.2.2 Elongation at break and work of fracture

The variation of elongation at break and work of fracture at test temperature ranging from -90℃ to 90℃ has been showed in Fig.6. Work of fracture was determined by calculating the area of force-displacement curve (F-D curve) with x-axial and the cross-sectional area of specimen.

The temperature effect of elongation at break and work of fracture shows a similar trend. For elongation at break, the effect is not monotonous. In low temperature, the elongation at break decreased with the temperature down. From 20℃ to -20℃, it had a drastic reduction. While high temperature increased elongation of the material because it increased the energy of molecular motion. In terms of the work of fracture, the maximum value appears at 20℃. The increase or decrease of temperature will lead to its reduction, which indicates higher temperature sensitivity in work of fracture.

It is worth noting that when temperature rises from 20℃ to 50℃, the elongation at break decreases by 22%. With the rise of test temperature, the elongation at break increases gradually. While the test temperature reached 90℃, the elongation at break exceed that at 20℃. The variation of work of fracture shows a similar trend. Considering that the glass transition of the tested material occurred below 51.9℃, according to the theory of free volume, the molecular chain segment had obtained enough motion energy and necessary free space, switching from frozen state to the motion state at T_g. In the glass transition

zone, the material is neither glassy state nor rubbery state. It has the characteristics of both elastic solid and viscous fluid, and has a great energy loss under the strain. The huge energy loss leads to the sudden reduction of elongation at break and work of fracture. Therefore, the mechanical properties of the material changed greatly from 20℃ to 50℃. Above the glass transition temperature, the free volume of the material is also involved in the expansion process caused by the high temperature. Both the elongation at break and the work of fracture are increasing as the further rise of test temperature.

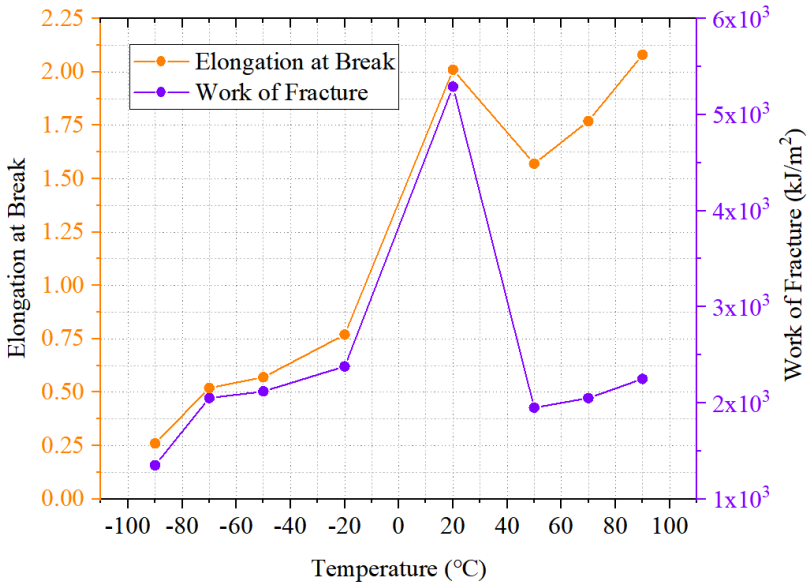

Figure 6. Curves of elongation at break and work of fracture at temperature ranging from -90℃ to 90℃

3.3 Weld seam effect

Fig.7 shows the weld seam effect on mechanical properties of PA6 at -70℃, -50℃ and 20℃. The tensile modulus is less affected by weld seam at each temperature. This is because the weld seam is a local defect which affects the local ability to resist deformation of the specimen, however, in tensile process, the deformation is uniform of whole specimen. Besides, the tensile strength, elongation at break and work of fracture are greatly affected by weld seam which means that the HAZ will be the initial crack location of the whole specimen due to the weakening effect of weld seam.

In addition, the mechanical weakening degree is related to the test temperature. The weld seam effect at 20℃ is larger than other two test temperatures. The degradation is very apparent for tensile strength, elongation at break and work of fracture, which is 28%, 58% and 67%, respectively. When temperature down from -50℃ to -70℃, the reduction of corresponding value becomes not sensitive to the temperature which is from 6.5% to 5.0%, 42% to 52% and 44% to 45%, respectively. However, tensile modulus at 20℃, -50℃ and -70℃ is decreased by 11%, 9.0% and 1.5%, respectively. All those values are around 10%.

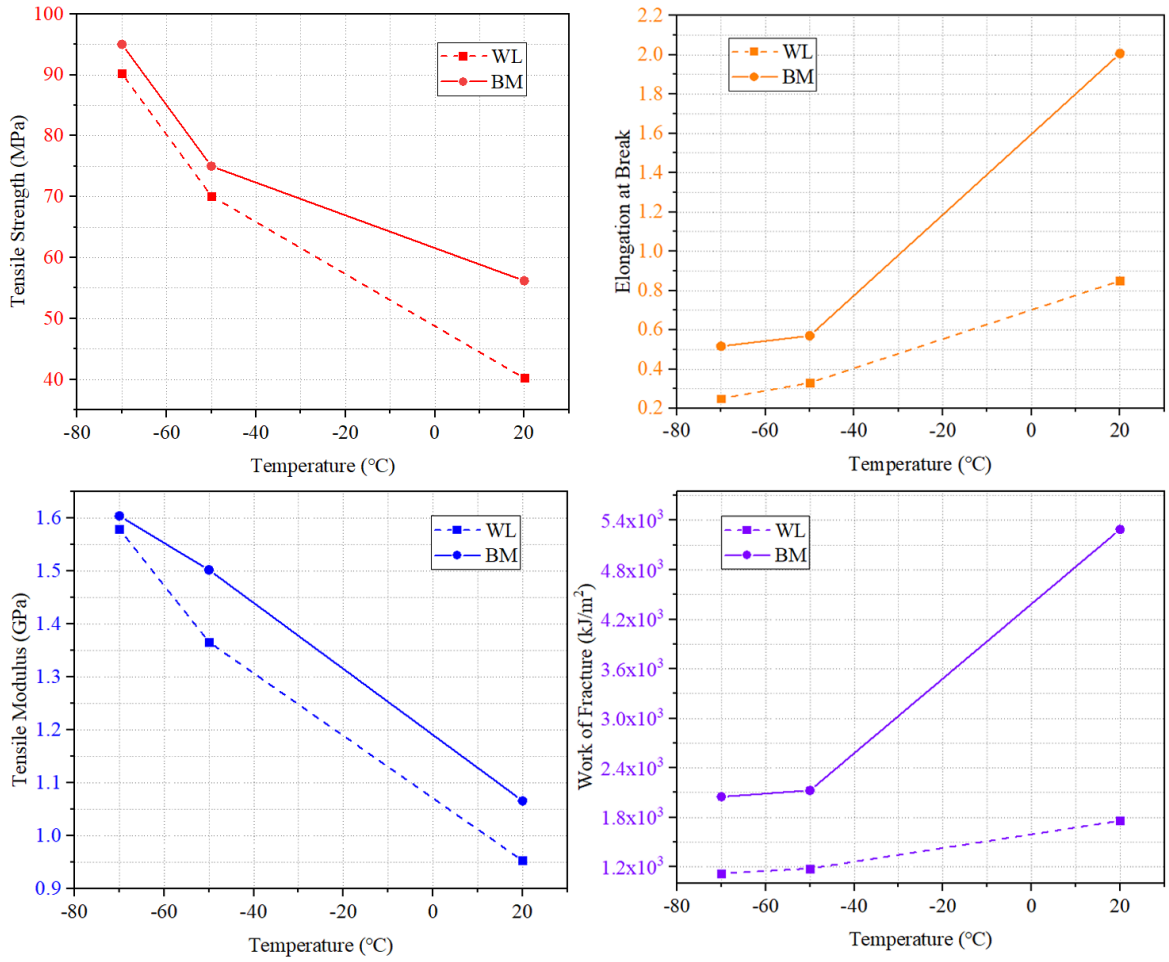

Figure 7. curves of weld effect on (a)tensile strength, (b)tensile modulus, (c)elongation at break and (d)work of fracture of PA6 at -70℃, -50℃ and 20℃.

3.4 Macroscopic structure

The overall morphology of the specimens after break is shown in Fig.8. The specimens elongated uniformly during the tension process with the formation of a large number of crazing. Compared with the clamped section, the stretched section is much whiter which is evidence of the generation of crazing. The whitening phenomenon is also affected by the temperature. The specimens with large deformation from -70℃ to 20℃ has obvious whitening phenomenon from the front and side view, while the whitening of the specimen at -90℃ and 50℃ to 90℃ is not obvious. It is because of the conditions of the lowest critical stress and critical elongation for the generation of crazing. The stress of the specimen at high temperature during the entire tensile process is relatively small, which is not conducive to the generation and development of crazing. Similarly, the specimen at -90 ℃ has a small elongation at break which cannot reach the critical elongation requirement of the generation of crazing.

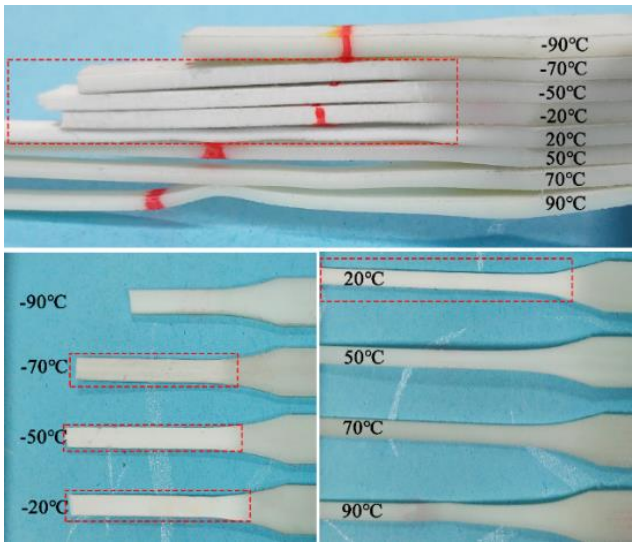

Figure 8. The whitening phenomenon of specimens at each test temperature.

Fig.9 shows the macroscopic fracture morphology of the fracture surface at each test temperature. The specimens in Fig.9(a), (b), (c), and (d) have a large reduction of the area of fracture surface. With the increase of temperature, the greater the roughness of the fracture surface, the greater the angle between the normal direction of fracture surface and the tensile direction. The specimens in Fig.9(e), (f), (g) and (h) have a small reduction of cross-sectional area, especially the specimen in Fig.9(e). With the decrease of temperature, the macroscopic fracture surface becomes more and more flat, which shows that the material becomes brittle gradually.

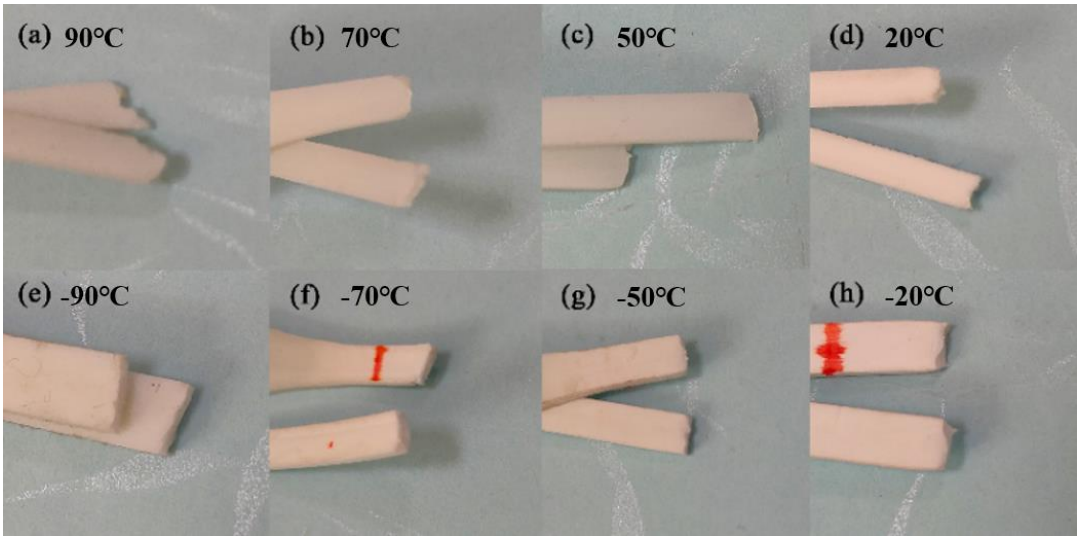

Figure 9. Macroscopic fracture morphology of specimens broke at test temperature of (a)90℃, (b)70℃, (c)50℃, (d)20℃, (e)-90℃, (f)-70℃, (g)-50℃, (h)-20℃.

3.5 Microscopic structure

Fig.10 shows the fracture surface morphology of specimens in low temperature of -90℃, -70℃, -50℃ and -20℃. The magnifications of SEM is ×23, ×27, ×27 and ×30, respectively. Analysis of the fracture surface shows that the temperature affects the size of each area (fiber area, radiation area and fracture area) of the fracture surface morphology. As the temperature decreases, the fiber area and radiation area shrink while the fracture area expands. This demonstrates that the low temperature weakens the toughness of the polyamide 6. In particular, radiation at -70 ℃ and -90 ℃ is not as neat as at -50℃ and

-20℃. What's more, the edge shape of the fracture surface has almost no shrinkage deformation at -90 ℃. This shows that when the temperature drops and reaches -90 ℃, the toughness of polyamide 6 decreases severely, and the amount of plastic deformation is greatly reduced.

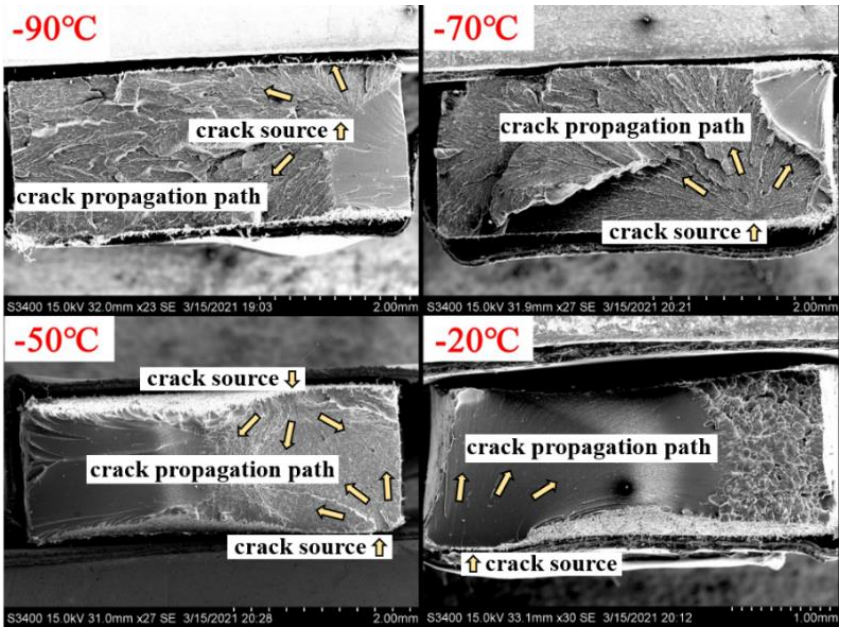

Figure 10. Fracture morphology of specimens in low-temperature tensile test under low magnification

Fig.11 shows the fracture surface morphology of specimens in low temperature of 90℃, 70℃, 50℃ and 20℃. The magnifications of SEM is ×37, ×35, ×32 and ×32, respectively. This magnification is slightly larger than that in low temperature because the fracture surface has a greater shrinkage rate when the specimen stretched at high temperature. In addition, compared with the low temperature, the high temperature does not significantly change the size of each area of the fracture surface morphology. The fiber area and radiation area expand slowly with the increase of temperature.

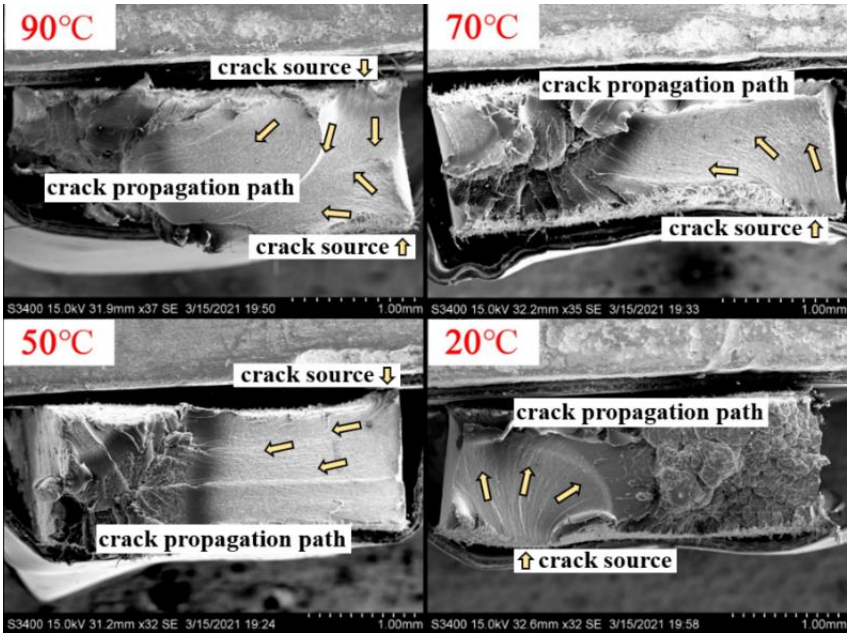

Figure 11. Fracture morphology of specimens in high-temperature tensile test under low magnification

Fig.12 shows the SEM images of two different microscopic structure of fracture surfaces. The microscopic structure of fracture surfaces at -20℃, 70℃ and 90℃ present a neat fibrous arrangement along the fracture direction. While the test temperature is at -90℃, the fracture morphology shows a different feature. The large areas of fibrous morphology disappeared and replaced by a flatter fish-scale morphology which is smoother and flatter than its counterpart. This demonstrates the toughness degradation of the polyamide 6 [26].

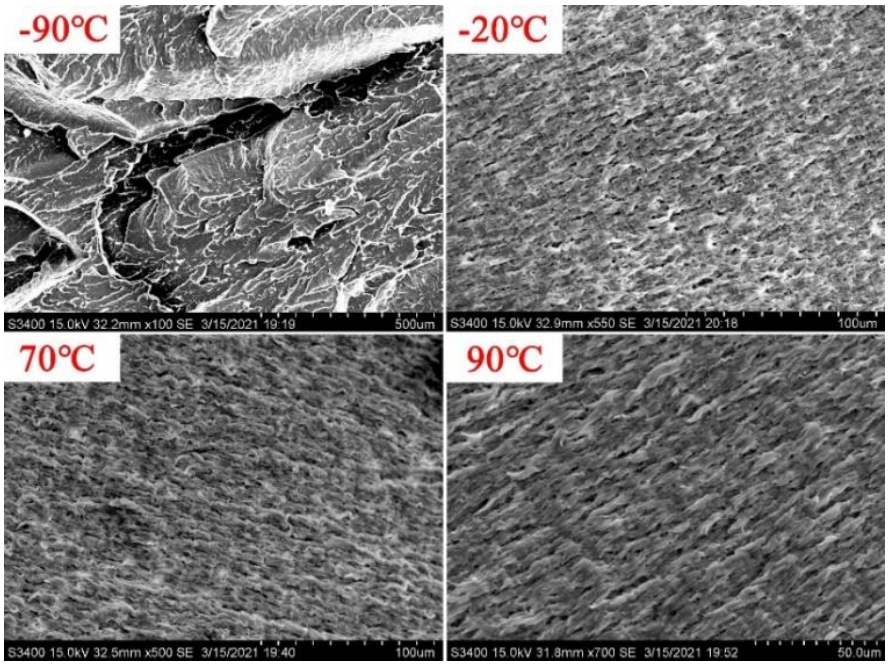

Figure 12. Two different Microscopic structure

The microscopic morphology of fracture surface of BM and WS specimens are showed Fig.13. The fracture surface of WS specimen is smooth, indicating that the crack propagate is not affected by any obstacles. The BM fracture surface is very rough, with ridges and valleys, and the cracks propagate toward different directions, accompanied by twists and tilts. The valleys on fracture surface and the deflection of cracks will consume more energy, therefore the material has a greater toughness [27].

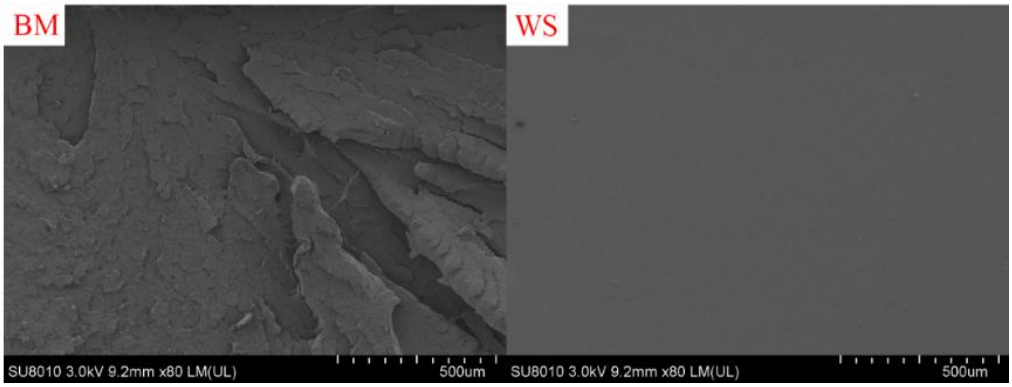

Figure 13. Microscopic morphology of fracture surface of BM and WS specimens

4.0 CONCLUSION

In this study, the temperature effect on the mechanical properties of polyamide 6 and the morphology and microstructure of fracture behaviour were investigated. The weld seam weaken effect was also clarified via contrastive analysis. The conclusions are drawn as follows:

- The influence of temperature on the tensile strength and tensile modulus of PA6 is close to a linear relationship. As temperature decreases, the tensile strength and tensile modulus increase, and reach the maximum at -90°C. This effect is greater in the range from 50°C to -90°C, and the tensile strength and tensile modulus are increased by 2.46 times and 10.6 times, respectively. For the elongation at break and work of fracture, the temperature effect is not monotonous. In low-temperature environment, as the temperature decreases, both of them are nearly linearly reduced. When the temperature rises from 20 ℃ to 50 ℃, both decreases, especially for work of fracture, reduced by 63%. As the temperature continues to rise, the elongation at break gradually increases, and returns to the level of 20 ℃, while the increase of work of fracture is not large, only 15%.

- The weld seam weakens those four mechanical properties of polyamide 6 specimens, and for the elongation at break and work of fracture, that effect is more obvious which is over 40% at each temperature. Among the test temperatures of -70°C, -50°C and 20°C, the degradation of tensile strength, tensile modulus, elongation at break and work of fracture is the largest at 20°C, which is 28%, 11%, 58% and 67%, respectively. Furthermore, it was found that the fracture surface of the WS specimen was flush, and was quite different from the toughness fracture of the BM specimen via SEM.

- The fracture behaviour of polyamide 6 can be judged from the S-S curve and the macroscopic and microscopic morphology of the fracture surface. In this test, the elongation at break from the S-S curves is all above 25%, and there is a strain hardening stage, which is the feature of ductile fracture. It can be observed from the macroscopic morphology of the fracture surface that as the temperature decreases, the roughness of the surface gradually decreases and tends to be flattened. As for the microscopic morphology, it can be found that the fracture surface at -90 ℃ and other temperatures show different morphologies, which is a sufficient evidence of low-temperature toughness degradation effect.

ACKNOWLEDGEMENT

This work was supported by the Key Research and Development Program of Zhejiang Province of China (No. 2020C01118).

REFERENCES

1. Mao Z.Q. and GAN Y. New development of hydrogen fuel cell vehicles. Solar Energy, 2012. 000(008): p. 17-22.
2. Li, L., et al., Review and outlook on the international renewable energy development. Energy and Built Environment, 2020.
3. Liu J. and Cui C. Breakthrough of hydrogen fuel cell vehicles. China Investment, 2017(19): p. 82-83.
4. Ahmad, M.S., M.S. Ali and N.A. Rahim, Hydrogen energy vision 2060: Hydrogen as energy Carrier in Malaysian primary energy mix – Developing P2G case. Energy Strategy Reviews, 2021. 35: p. 100632.
5. Wilberforce, T., et al., Developments of electric cars and fuel cell hydrogen electric cars. International Journal of Hydrogen Energy, 2017. 42(40): p. 25695-25734.
6. Singh, R., M. Singh and S. Gautam, Hydrogen economy, energy, and liquid organic carriers for its mobility. Materials Today: Proceedings, 2020.
7. Turoń, K., Hydrogen-powered vehicles in urban transport systems – current state and development. Transportation Research Procedia, 2020. 45: p. 835-841.
8. Wang, D., et al., Development of regulations, codes and standards on composite tanks for on-board gaseous hydrogen storage. International Journal of Hydrogen Energy, 2019. 44(40): p. 22643-22653.
9. Ortiz Cebolla, R., et al., Hydrogen tank first filling experiments at the JRC-IET GasTeF facility. International Journal of Hydrogen Energy, 2014. 39(11): p. 6261-6267.

10. Melideo, D., et al., CFD model performance benchmark of fast filling simulations of hydrogen tanks with pre-cooling. International Journal of Hydrogen Energy, 2014. 39(9): p. 4389-4395.
11. De Miguel, N., et al., The effect of defueling rate on the temperature evolution of on-board hydrogen tanks. International Journal of Hydrogen Energy, 2015. 40(42): p. 14768-14774.
12. De Miguel, N., et al., Compressed hydrogen tanks for on-board application: Thermal behaviour during cycling. International Journal of Hydrogen Energy, 2015. 40(19): p. 6449-6458.
13. Li, M., et al., Review on the research of hydrogen storage system fast refueling in fuel cell vehicle. International Journal of Hydrogen Energy, 2019. 44(21): p. 10677-10693.
14. Liu, J., et al., Numerical study on the fast filling of on-bus gaseous hydrogen storage cylinder. International Journal of Hydrogen Energy, 2020. 45(15): p. 9241-9251.
15. Xiao, J., et al., Final hydrogen temperature and mass estimated from refueling parameters. International Journal of Hydrogen Energy, 2018. 43(49): p. 22409-22418.
16. Baek, K., et al., Multiscale study for the temperature effect on the mechanical properties and fatigue crack growth rate of polyamide 66. Extreme Mechanics Letters, 2021. 43: p. 101154.
17. Felder, S., et al., Modeling the effect of temperature and degree of crystallinity on the mechanical response of Polyamide 6. Mechanics of Materials, 2020. 148: p. 103476.
18. Cano, A.J., A. Salazar and J. Rodríguez, Effect of temperature on the fracture behaviour of polyamide 12 and glass-filled polyamide 12 processed by selective laser sintering. Engineering Fracture Mechanics, 2018. 203: p. 66-80.
19. Parodi, E., L.E. Govaert and G.W.M. Peters, Glass transition temperature versus structure of polyamide 6: A flash-DSC study. Thermochimica Acta, 2017. 657: p. 110-122.
20. Wolf, M., J. Werner and D. Drummer, Weld seam morphology and bond strength of infrared and vibration welded SLS parts of polyamide 12 as a function of the layer build-up direction and the welding process. Additive Manufacturing, 2020. 36: p. 101451.
21. Rhricht, M.L., et al., Correlation between weld seam morphology and mechanical properties in laser transmission welding of polypropylene. Procedia CIRP, 2020. 94: p. 691-696.
22. Dahiya M S , Khasa S , Agarwal A . Optical absorption and heating rate dependent glass transition in vanadyl doped calcium oxy-chloride borate glasses[J]. Journal of Molecular Structure, 2015, 1086:172-178.
23. Schawe, EK Jürgen. Measurement of the thermal glass transition of polystyrene in a cooling rate range of more than six decades[J]. Thermochimica Acta, 2015, 603:128-134.
24. Park, H., et al., Toward the constitutive modeling of epoxy matrix: Temperature-accelerated quasi-static molecular simulations consistent with the experimental test. Composites Part B: Engineering, 2018. 142: p. 131-141.
25. Pepin, J., et al., Determination of key parameters responsible for polymeric liner collapse in hyperbaric type IV hydrogen storage vessels. International Journal of Hydrogen Energy, 2018. 43(33): p. 16386-16399.
26. Zhou, G., W. Wang and M. Peng, Molecular-level dispersion of rigid-rod sulfonated aromatic polyamides in epoxy resin for extraordinary improvement in both strength and toughness. Polymer, 2018. 163: p. 20-28.
27. Faber, K.T. and A.G. Evans, Crack deflection processes—I. Theory. Acta Metallurgica, 1983. 31(4): p. 565-576.